

Time Domain Computation of a Nonlinear Nonlocal Cochlear Model with Applications to Multitone Interaction in Hearing

Jack Xin, Yingyong Qi[†], Li Deng[‡]

Abstract

We study a nonlinear nonlocal cochlear model of the transmission line type in order to understand the multitone interactions and resulting tonal masking effects. This requires computing solutions in the time domain, marching solutions in time to reach a multi-frequency quasi-steady state. Our model has both basilar membrane (BM) elastic damping and selective longitudinal fluid damping. The former is nonlinear and nonlocal in BM displacement, and plays a key role in capturing tonal interactions. The latter is active only near the exit boundary (helicotrema), and is built in to remove dispersion of long waves that causes growth of solutions there. Such boundary instability is absent in the frequency domain calculation for a single tone. We compute model solutions with a semi-implicit second order finite difference method, and illustrate numerically long wave dispersion phenomenon. We show numerical results on two tone suppression from both high and low sides, consistent with known behavior of two tone suppression. We then demonstrate numerically tonal masking effect among three tones, or how the fixed two tones are suppressed as we vary the third tone in frequency and amplitude. We observe qualitative agreement of our model solutions with existing cat auditory neural data.

Department of Mathematics and TICAM, University of Texas at Austin, Austin, TX 78712, USA. Corresponding author, email: jxin@math.utexas.edu. This work was partially supported by ARO grant DAAD 19-00-1-0524.

[†]Qualcomm Inc, 5775 Morehouse Drive, San Diego, CA 92121, USA.

[‡]Microsoft Research, One Microsoft Way, Redmond, WA 98052, USA.

1 Introduction

Cochlear modeling has had a long history, and it has been realized that nonlinearity is essential for multi-tone interactions, [1, 14, 2, 8] among others. The nonlinearity could be incorporated through micro-mechanics of cochlear, such as coupling of BM to inner hair cells [13, 17]. Alternatively, nonlinearity could be introduced phenomenologically based on spreading of electrical and neural activities between hair cells at different BM locations suggested by experimental data [12, 3]. The latter approach turned out to be rather efficient and will be adopted in this paper. Their model with nonlinear and nonlocal BM damping will be our starting point.

Multi-tone interaction requires one to perform numerical simulation and analysis in the time domain as the resulting time dependent problem is strictly speaking irreducible to a steady state problem. We found that the commonly used cochlear models, including those of Jan and Geisler [12], Deng [3], are intrinsically dispersive. In particular, long waves tend to propagate with little decay from entrance point (stapes) all the way to exit boundary point (helicotram a). Such an issue does not occur in the single tone case for which a reduction to the steady state is possible (or a frequency domain calculation) by factoring out the time dependence of solutions. This phenomenon prompted us to incorporate a selective fluid longitudinal damping term in the model of Jan and Geisler [12], Deng [3], operating near exit boundary (helicotram a). The role of such a term is to suck out the long waves accumulating near the exit.

We then present a second order semi-implicit finite difference method of our model. The method relaxes the stability time step constraint of explicit methods without going into the complexity of fully implicit schemes. As our model is nonlocal and nonlinear, semi-implicit scheme is a reasonable option for computation. Numerical examples showed that the method is efficient, and that the selective damping term indeed removes the long waves at the exit boundary point for a time domain calculation of a single tone. The examples also demonstrated that the analysis of dispersive waves and slow decay of long waves is robust, and the phenomenon persists in the nonlinear nonlocal regime of the model.

Subsequently, we show computational results on isodisplacement curves for five characteristic frequencies consistent with those of Neely [20] for BM displacement of 1 nm. In case of two tone interactions, our model gives both low and high side suppression, in qualitative agreement with similar studies of Geisler [8]. For understanding three tone interactions, we fix the frequencies and amplitudes of two tones, and vary the third tone both in frequency and amplitude in a manner similar to auditory neural experiment of Deng and Geisler [4]. Again, our model showed masking of the two tones by the third tone, in qualitative agreement with experimental data. The stage is set for further study of our model on more complicated tones.

The rest of the paper is organized as follows. In section 2, we present our model and its background, also analysis of dispersive properties of solutions. In section 3, we outline our semi-implicit discretization of the model. In section 4, we give model parameters, and show numerical results on dispersion of model solutions, isodisplacement curves, two and three tone interactions in comparison with existing data. The conclusions are in section 5.

2 Nonlinear Nonlocal Cochlear Model

2.1 Background and Model Setup

The cochlear modeling has had a long history driven by advancement of cochlear experiments, see [24, 21, 1, 8] among others. A brief derivation of the one dimensional (1-D) cochlear model of transmission line (long wave) type, based on fluid mechanics and elasticity, can be found in Sondhi [22], see also references therein for earlier contributions, and [2] for later development and higher dimensional models. A general form of the 1-D model can be expressed as:

$$p_{xx} - N u_{tt} = -s u_t; \quad x \in (0; L); \quad (2.1)$$

$$p = m u_{tt} + r(x; u) u_t + s(x) u; \quad (2.2)$$

where p is the fluid pressure difference across the basilar membrane (BM), u the BM displacement, L the longitudinal length of BM; stapes is at $x = 0$, and helicotrema is at $x = L$; N a constant depending on fluid density and cochlear channel size; s depends on the damping of longitudinal fluid motion [18]; m , r , s are the mass, damping, and stiffness of BM per unit area, with m a constant, s a known function of x , and r a function (all) of x , u .

Choosing a functional form for r is a key step in model design. Most choices in the literature assume that r is a local nonlinear function, [11, 7, 25, 13, 2]. The nonlinearity is necessary to model two tone nonlinear interaction (e.g. two tone suppression effects). However, as pointed out by Kim [14], local form of r is not sufficient to account for two tone suppression when suppressors are below the excitors in frequency (low side), unless a "second filter" is incorporated, see e.g. [11]. To achieve the second filter effect on more physical grounds, micromechanical approaches have been developed to derive damping r from motion of outer hair cells and other physiologically relevant parts of cochlear, [14, 25, 2, 17] among others. Though this is a reasonable approach, one faces the daunting complexity of the cochlear micromechanics, see [17] for recent progress along this line. Lim [17] showed that 2-D micromechanical models capture both high and low side two tone suppression, in agreement with BM experimental data. The alternative approach, first proposed in this context by Jau and Geisler [12], is a bit more phenomeno-

logical in nature. It hypothesized that there is longitudinal coupling in the cochlear partition itself, and damping r is a convolution integral of u with an exponential weight function on BM. Similar idea appeared also in Lyon [19] in coupled automatic gain control framework. Possible physiological mechanisms underlying the spatially coupled nonlocal damping were identified in Deng [3], and the resulting model was then used to process acoustic signals.

We shall adopt the latter nonlocal damping approach for choosing the function r . The BM damping coefficient is specified as in Jau and Geisler [12], Deng [3]:

$$r(x;t;u) = r_0(x) + \int_0^{Z_L} \mu(x^0;t) \exp[-\beta(x-x^0)^\alpha] g dx^0; \quad (2.3)$$

where $r_0(x)$ is the passive BM damping; μ and β are positive constants. The size of r controls how sharp the BM traveling wave envelope would be. One could in principle add on another so called locally active damping term, e.g, a term like $a(1 - \exp[-b|x-L|]) = \mu_t$; $a, b > 0$, as suggested in [25], however, we found in our numerical experiment that the nonlocal term in (2.3) is far more effective just by itself.

We shall take s as a function of x so that $s = s(x) = 0$ is a smooth function and is supported near the vicinity of $x = L$, for instance:

$$s(x) = \frac{1}{1 + \exp[-(x_1 - x)^\gamma]}; \quad (2.4)$$

where x_1 is slightly smaller than L ; $\gamma > 1$, $\beta > 1$, are two constants, with β suitably large. In existing works, s has been either zero throughout $x \in (0;L)$, see [7, 3, 25] or a function of both signs for constructing a stable active model without a second tuned structure, see [18]. Taking s as a spatially dependent function can be considered as a way to selectively introduce damping so that possible low frequency waves near $x = L$ are damped out and there is minimal wave accumulation (or reflection) close to the helicotrema (at $x = L$). This turns out to be an essential stabilizing mechanism for our time domain numerical computation. We will come back to this point later.

The coefficients m , n , and $s(x)$ are standard. The function $s(x)$ is based on the data of [15]. The physical boundary and initial conditions are:

$$p_x(0;t) = T_M p_T(t); \quad p(L;t) = 0; \quad (2.5)$$

$$u(x;0) = u_t(x;0) = 0; \quad (2.6)$$

where $p_T(t)$ is the input sound pressure at the eardrum; and T_M is a bounded linear operator on the space of bounded continuous functions, with output depending on the frequency content of $p_T(t)$. If $p_T = \sum_{j=1}^P A_j \exp[i\omega_j t + c.c.]$, a multitone input, $c.c$ denoting complex conjugate,

then $T_M p_T(t) = \sum_{j=1}^P B_j \exp(i\omega_j t + \alpha_j x)$, where $B_j = a_M(\omega_j) A_j$, $a_M(\omega)$ is a scaling function built from the filtering characteristics of the middle ear. Established data are available in Guinan and Peake [10]. The model setup is now complete.

2.2 Model Properties and Analysis

We briefly go over some special regimes and solutions of the model system to illustrate the basic mathematical properties and issues. If $m = 0, r = 0, \gamma = 0$, (2.1)-(2.2) reduces to a second order wave equation: $nu_{tt} - (s(x)u)_{xx} = 0$. When γ is turned on, and $\gamma = 0$, we have a damped second order wave equation driven by boundary condition at $x = 0$. Now suppose that all coefficients are constants, then (2.1)-(2.2) considered on the entire line admits planar wave solutions of the form:

$$u = u_0 \exp(i(kx - \omega t)); p = p_0 \exp(i(kx - \omega t));$$

where k is the spatial wave number, ω the temporal frequency; u_0 and p_0 are respectively the amplitude of displacement and pressure. Upon substitution, it follows that:

$$\begin{aligned} p_0 &= (m\omega^2 - i\gamma\omega + s)u_0; \\ (k^2m + N)\omega^2 + i(k^2r + \gamma)\omega - s^2 &= 0; \end{aligned} \quad (2.7)$$

If the damping coefficients $r = \gamma = 0$, then:

$$\omega = \frac{ks_0^{1/2}}{(k^2m + N)^{1/2}}; \quad (2.8)$$

showing that the system is dispersive, see [26], i.e., $\omega = \omega(k)$ and $\omega'(k) \neq 0$. Waves of different wave length ($\lambda = 2\pi/k$) travel at different velocities. The dispersion relation (2.8) gives the group velocity:

$$\omega'(k) = \frac{1}{2} \frac{s_0^{1/2}}{(k^2m + N)^{3/2}}; \quad (2.9)$$

which decays to zero as $k \rightarrow \infty$. In other words, short waves (k large) do not disperse as fast as long waves (k small).

When damping coefficients $r, \gamma > 0$ ($\gamma = 0$), we have a damped dispersive system, (2.8) is modified into:

$$\omega = \frac{i(k^2r + \gamma) \pm \sqrt{4s_0k^2(k^2m + N) - (k^2r + \gamma)^2}}{2(k^2m + N)}; \quad (2.10)$$

with $\text{Im } \omega = -(k^2r + \gamma)/2(k^2m + N) < 0$, leading to decay of planar waves. The decay rate $\text{Im } \omega$ shows that if $\gamma = 0$, the decay of long waves ($k \rightarrow 0$) is very slow, with rate of order $O(k^2)$. Hence the decay of long waves relies entirely on γ .

We remark that the cochlear model in [3, 6] also contains a so called stiffness coupling term in equation (2.2), so the elastic response becomes: $p = m u_{tt} + r(x; t; u)u_t + s(x)u - K(x)u_{xx}$; for some positive function $K(x)$, rendering the highest spatial derivative order four in the model. Nevertheless, it is easy to check that the additional term does not change the dispersive nature of model solutions, neither the long wave dispersion and slow decay properties.

As we will see, the long wave dispersion and slow decay properties persist when coefficients become variables, and could cause problems for numerics. However, the generic dispersive effect of the time dependent solutions is absent in the special case when the temporal dependence of solution can be factored out. This is the case when the input $P_T(t)$ is a single tone, or in complex variables $P_T(t) = A \exp(i\omega t + i\kappa x)$. Writing solution as $u = U(x) \exp(i\omega t + i\kappa x)$, $p = P(x) \exp(i\omega t + i\kappa x)$, we derive the following boundary value problem:

$$P(x) = (m\omega^2 + ir(x; \omega))U; \tag{2.11}$$

$$P_{xx} + (N(x) - \kappa^2)U = 0; \tag{2.12}$$

subject to the boundary conditions:

$$P_x(0) = T_M A; P(L) = 0; \tag{2.13}$$

This is the way frequency domain calculation for single tones is done, turning a time dependent problem into a steady state problem on wave amplitudes, avoiding transients and the dispersion effect. However, for multiple tones, it is impossible to factor out the time dependence exactly. For approximate procedures (some kind of quasi-steady approximation) in frequency domain for studying two tone interactions, see [13, 17]. To do an accurate computation directly on system (2.1)–(2.6), one has to proceed in the time domain, or solving the initial boundary value problem in time until transients die out and solutions approach a limiting time dependent state (quasiperiodic in time for multiple tones), similar to invariant tori in Hamiltonian mechanics. It is a very interesting mathematical problem to (1) construct such "invariant tori" for a damped driven dispersive system like our cochlear model; (2) find an iterative scheme for approximation and analyzing the approximation error. As a first step, one needs to analyze the nonlinear nonlocal steady state problem (2.11)–(2.13) for single tone (limit cycle case), establishing an existence and uniqueness theorem, this is currently in progress [27].

3 Numerical Method

In this section, we discuss our numerical method for solving system (2.1)–(2.6) and related numerical issues. Solutions of cochlear model with tonal inputs behave like traveling waves

during early time, and eventually settle down to time periodic states of different periods at various BM locations according to the resonance information (frequency to place mapping) encoded in the function $s(x)$. A time domain computation will provide the stabilized limiting multi-frequency oscillating states after a long enough time integration. An ideal numerical method would be one that can reach the limiting states with accuracy, low cost and speed.

Let us first briefly review some existing methods. For a cochlear model with locally nonlinear damping function r (van der Pol type), a method of line discretization is implemented in [7]. Discretization in space is a Galerkin finite element method (of second order, with piecewise linear basis), and time stepping is explicit variable step 4th order Runge-Kutta, found to be superior to earlier explicit time stepping schemes such as Heun's and modified Sielecki methods. A fully discrete explicit finite difference discretization, first order in time 2nd order in space, is carried out in [3, 6]. The discretization can be viewed as central differencing in space and forward Euler in time. The explicit nature of these methods put a severe stability constraint on the time step, requiring long computation time to reach stable quasi-periodic states that we are most interested in. Also it is known that one step explicit methods like Runge-Kutta, Heun and Euler, are prone to accumulation of truncation errors for approximating dynamic objects like limit cycles, see [9], chapter 2.

Though implicit methods typically relax the stability constraints on time step and are better for computing steady states, they are also likely to be slow due to Newton iteration at each time step, and the non-banded complicated Jacobian matrix as a result of the nonlocal damping term. When r is only Lipschitz continuous in u , lack of smoothness is another concern for the condition of the associated Jacobian matrix. This motivates us to look into semi-implicit methods that allow larger time steps and better stability properties than explicit methods, while being cheaper and faster than fully implicit schemes.

Let us introduce our 2nd order accurate semi-implicit discretization. We denote by u_j^n (p_j^n) the numerical approximation of solution $u(jh; nk)$ ($p(jh; nk)$), where h the grid size for $x \in [0; L]$, k the time step. Let δ_{jh} be the forward/backward finite differencing operator in x , δ_{jk} the forward/backward finite differencing operator in t . Central first differencing operator in space is $\delta_{jh} = \frac{\delta_{jh}^+ - \delta_{jh}^-}{2}$, and central second differencing operator in space is $\delta_{jh}^2 = (\delta_{jh}^+ \delta_{jh}^-) = h^2$; with similar notations δ_{jk}^2 for central differencing operator in time. The semi-implicit method for system (2.1-2.6) is:

$$N \delta_{jk}^2 u_j^n = \frac{1}{4} \delta_{jh}^2 (p_m^{n+1} + 2p_m^n + p_m^{n-1}) - j_{0;k} u_j^n; \quad (3.1)$$

$$p^{n+1} = m \frac{2u_j^{n+1} - 5u_j^n + 4u_j^{n-1} - u_j^{n-2}}{k^2} + r_j^n (u_t)_j^{n+1} + s_j u_j^{n+1}; \quad (3.2)$$

where $1 \leq j \leq J, n \geq 2$, and:

$$r_j^n = [r_{0,j} + h(\frac{1}{2}j_1^{n+1}j_1^{n+1} + \frac{1}{2}j_j^{n+1}j_j^{n+1} + \sum_{l=2}^{j-1} j_l^{n+1}j_l^{n+1})]; \quad (3.3)$$

where $(u_t)_j^{n+1}$ is approximated at second order by:

$$\begin{aligned} (u_t)_j^{n+1} &= (u_t)_j^n + (2k)(u_{tt})_j^n + O(k^2) \\ &= u_{0,k}u_j^n + \frac{2k}{N}((p_{xx})_j^n - j(u_t)_j^n) + O(k^2) \\ &= u_{0,k}u_j^n + \frac{2k}{N}(h^2p_j^n - j u_{0,k}u_j^n) + O(k^2); \end{aligned} \quad (3.4)$$

and:

$$\begin{aligned} j_1^{n+1}j_1 &= j_1^n + k(u_t)_1^n + O(k^2)j_1 \\ &= j_1^n + (4u_1^{n-1} - u_1^{n-2} - 3u_1^n) = (2)j_1 + O(k^2) \\ &= j_1(4u_1^{n-1} - u_1^{n-2} - 5u_1^n) = (2)j_1 + O(k^2); \end{aligned} \quad (3.5)$$

In (3.4), we have used the equation (2.1) once to lower time derivative of u by one order. In (3.2), (3.3) and (3.5), we have also used one sided second order differencing to approximate u_{tt} , u_t , and trapezoidal rule to approximate the spatial integral. The variables at $t = (n+1)k$ are all linear. It follows from (3.2) that:

$$u_j^{n+1} = \frac{k^2 p_j^{n+1} - m(5u_j^n + 4u_j^{n-1} - u_j^{n-2}) + kr_j^n(4u_j^n - u_j^{n-1})}{2m + 3kr_j^n + k^2 s_j}; \quad (3.6)$$

Substituting (3.6) into (3.1) to eliminate u^{n+1} , we get the following linear system of equations on p^{n+1} ($h = k$):

$$\begin{aligned} [(N + \frac{jk}{2})k^2 + (2m + \frac{3kr_j^n}{2} + k^2 s_j)] p_j^{n+1} + \frac{2}{4} p_{j+1}^{n+1} + \frac{2}{4} p_{j-1}^{n+1} \\ = N(2u_j^n + u_j^{n-1}) + (N + \frac{jk}{2}) \frac{m(5u_j^n + 4u_j^{n-1} - u_j^{n-2}) + \frac{kr_j^n}{2}(4u_j^n - u_j^{n-1})}{(2m + \frac{3kr_j^n}{2} + k^2 s_j)} \\ - \frac{2}{4} [2(p_{j+1}^n - 2p_j^n + p_{j-1}^n) + p_{j+1}^{n-1} - 2p_j^{n-1} + p_{j-1}^{n-1}] - \frac{jk}{2} u_j^{n-1}; \end{aligned} \quad (3.7)$$

which is solved by inverting a diagonally dominant tridiagonal matrix. Once p^{n+1} is computed, u^{n+1} is updated from (3.6).

The first two time steps are initiated as follows. Initial condition, (2.1), and (2.2) give:

$$p_{xx} = \frac{N}{m} p = 0; \quad p_x(0) = f(0); \quad p(L;0) = 0;$$

whose solution is:

$$p(x;0) = \frac{f(0)}{N} \frac{1 - e^{-\frac{q}{m}x}}{1 + e^{-\frac{q}{m}2L}} \exp\left(\frac{q}{m}x\right) \quad (3.8)$$

At $t = k$, we found

$$u(x;k) = k^2 u_{tt} + O(k^3) = \frac{k^2}{2m} p(x;0) + O(k^3);$$

and similarly:

$$u_t(x;k) = kp(x;0) + k^2 u_{ttt}(x;0) + O(k^3);$$

To find $p(x;k)$, denote $q(x) = p_t(x;0) = m u_{ttt}(x;0) + r(x;0)u_{tt}(x;0)$. It follows from (2.1) that $q_{xx} - \frac{N}{m}q = -r(x)u_{tt}(x;0)$, implying

$$q_{xx} - \frac{N}{m}q = -r(x)u_{tt}(x;0) - \frac{N}{m}r(x;0)u_{tt}(x;0);$$

or a uniquely solvable two point boundary value problem on q :

$$q_{xx} - \frac{N}{m}q = -N r(x;0)u_{tt}(x;0) - \frac{N}{m}r(x;0)u_{tt}(x;0); \quad (3.9)$$

with boundary condition: $q_x(0) = f'(0)$, $q(L) = 0$.

It follows then from the definition of q that:

$$\begin{aligned} u_{ttt}(x;0) &= q(x) - r(x;0)p(x;0); \\ u_t(x;k) &= kp(x;0) + \frac{k^2}{2} (q(x) - r(x;0)p(x;0)); \end{aligned} \quad (3.10)$$

Equations (2.1)-(2.2) at $t = k$ implies the uniquely solvable two point boundary value problem on $p(x;k)$:

$$p_{xx} - \frac{N}{m}p = -r(x)u_{tt}(x;k) - N s(x)u; \quad (3.11)$$

with boundary condition: $p_x(0) = f(k)$, $p(L) = 0$. Both (3.9) and (3.11) are solved with a standard second order discretization. We then will have computed $(u;p)(x;k)$. Similarly, with k replaced by $2k$, we compute $(u;p)(x;2k)$.

The left boundary condition $p_x(x;0) = f(t)$ is discretized as: $p_2^{n+1} - p_0^{n+1} = 2hf((n+1)k)$, with second order accuracy. The right boundary condition $p_{J+1}^{n+1} = 0$ is exact. The semi-implicit method is now completely defined, and it reduces to an unconditionally stable implicit method for standard second order wave equation when $m = 0$, s is constant, and damping is absent, [23], chapter 8.

4 Numerical Results and Multitone Interaction

In this section, we present numerical results based on our model and numerical methods discussed in the last two sections. First we list all parameters of our cochlear model and those of the associated middle ear model based on Guinan and Peake [10]. We then show computed single tones and demonstrate the dispersion effects of long waves and the role of selective longitudinal fluid damping in our model. As a test of model tuning property, we also show the computed isodisplacement curves (at characteristic frequencies 500 Hz, 2 kHz, 4 kHz, 6 kHz, 10 kHz). Subsequently, we give numerical examples of both the high side and low side suppression of two tone interaction in model solutions consistent with Figures 10.2, 10.4, 10.7 in [8]. The asymmetry of high and low side suppression is captured by the model. We then show numerical simulation of three tone interaction, presenting results on how the amplitudes of the two of the three tones change as we vary the amplitude and frequency of the third tone, qualitatively consistent with experimental data of Deng and Geisler [4] on responses of auditory neural fibers to input of three tones.

4.1 Model Parameters

The parameters for (2.2) are: cochlear length 3.5 cm; mass density 0.05 cm^{-3} ; $\beta = 0.2$; $\gamma = 0.2 \text{ cm}^{-1}$; $N = 16.67 \text{ (dyne-cm}^{-3}\text{)}$; $r_0 = 0.001 \text{ g-cm}^{-2}\text{m s}$; and

$$s(x) = (4 \text{ })^2 m (0.456 \exp(4.83(1 - x/3.5)) - 0.45)$$

following [15].

The middle ear serves as a low (high) pass filter from sound pressure at eardrum to the displacement (acceleration) of stapes. We fit the data in [10] with the following gain factor $a_M(\omega)$ for each input $e^{i\omega t}$:

$$a_M(\omega) = 30 \left(\frac{1}{30} + 0.0605 \omega^2 \left(1 + \frac{\omega^2}{\omega_m^2} \right)^2 + (2 \omega \omega_m - \omega_m^2)^2 \right)^{-1/2}; \quad (4.1)$$

where $\omega_m = 4 \text{ kHz}$, the middle ear characteristic frequency, $\gamma_m = 0.7$ the middle ear damping ratio.

4.2 Dispersion Effect

We illustrate the dispersion property of time dependent solutions numerically in case of one tone input. In top plot of Fig. 1, we show the profiles of computed traveling wave at $t = 16$

ms with and without the selective damping term, $(x)u$. For the run, $h = 0.01$, $k = 0.01$, and $x_1 = 3$, $\alpha = 4$. We see that for a tone input of 4kHz, 50dB, without selective damping, the BM displacement at $t = 16$ ms contains a long wave which manages to pass through the characteristic location in the interval (1.5;2) and persists near the exit $x = L$. This is due to the dispersive long waves with slow decay as we demonstrated analytically in the last section. In contrast, when the selective damping term is present, the long wave is damped as it moves close to the right end point $x = L$. As the selective damping term is only effective near $x = L$, the solutions in the interior of the domain are essentially the same. In the bottom plot of Fig. 1, we show the BM displacement at $t = 32$ ms, the dispersive long wave persists. In other runs (not shown here), we also observed growth in amplitude of long waves near $x = L$ with time at a linear rate. The appearance of long waves seems to be independent of numerical methods, rather their existence is intrinsic to the model which is dispersive. However, such an effect is much weaker in BM velocity output. In Fig. 2, we plot the BM velocities at $t = 16$ ms and 32 ms, the dispersive long waves are nearly negligible; this also indicates that the dispersive long wave growth is linear or sublinear. In existing papers on time domain calculations, [7, 6, 25] among others, such behavior was not noticed and analyzed. From a theoretical perspective, however not in the context of time domain computations, [16] discussed the dispersive aspect of linear cochlear models.

4.3 Numerical Parameters

For all our runs reported below, $h = k = 0.01$, $\alpha = 500$, $\beta = 4$, $x_1 = 3$. The x_1 and α values should be properly increased (x_1 closer to $x = 3.5$) if there are low frequencies below 300Hz in the input frequencies. Smaller h and k values have been used to test that numerical solutions do not vary much with further refinement. The time step k should be made suitably smaller if input frequencies are as large as 16kHz for more resolution.

4.4 Isodisplacement Tuning Curves

In Fig. 3, we show model isodisplacement curves for five characteristic frequencies 500 Hz, 2 kHz, 4 kHz, 6 kHz, 10 kHz. The threshold displacement is 1 nm. The curves showed the trend of sharper peaks in high frequencies, wider peaks for lower frequencies, and the asymmetry about the peak points. The plot is comparable to the one in [20]. In Fig. 4, we compare the tuning curves with and without the nonlinearity at 2 kHz, 4 kHz, 6 kHz, to illustrate the role of nonlinearity. We see that nonlinearity lowers the threshold intensities and sharpens peak regions, away from which the nonlinear effect is weak. This is expected since the tuning curves

are obtained using relatively low sound pressure levels (SPLs) and hence the nonlinear effects are low.

4.5 Two and Three Tone Interactions

Two tone interaction is well-documented in the literature, here we illustrate that our model gives qualitatively the same results as shown in related figures in [8]. We shall use BM displacement to detect the tonal interaction. Fig. 5 shows that the amplitude of a 5 kHz 70 dB tone (solid line) drops by nearly 50% after the second tone of 2.4 kHz and 70dB is introduced (dot-line), this reveals the so called low side suppression. When both tones are at 50dB, the 5 kHz tone (solid line) is still suppressed though by a much less percentage (10% or so) in the presence of the 2.4 kHz tone (plus-line), as illustrated in Fig 6. In view of isodisplacement plot 3, if we regard 1 nm as corresponding to hearing threshold value as [8], 50dB of 2.4 kHz is located below the tuning curve at characteristic frequency 5 kHz (unplotted in Fig. 3 but in between the tuning curves at characteristic frequencies 4kHz and 6kHz), and 50 dB of 5kHz is just above the threshold. This is the classical regime of low side two tone suppression, see [8] (Figure 10.4, and Figure 13.9).

In Fig. 7, we see that the 5 kHz tone at 50 dB (solid line) is suppressed by about 30% after interacting with 6.7 kHz tone at 80 dB (plus-line), the so called high side suppression. The high side suppressor tone at 6.7 kHz has to be much higher in amplitude than a low side suppressor tone whose frequency is at least as far away from that of the suppressed tone. In Fig. 8, we see that if the amplitude of the 6.7 kHz tone is reduced to 50 dB, there is no suppression effect anymore. In contrast, the 50 dB 2.4 kHz tone has suppression ability still in Fig. 6. This clearly demonstrates the asymmetry of low and high side suppression as is known, see [8] among others.

Now we consider the effect of adding a third tone to a pair of two tones (4 kHz, 4.4 kHz), all at 50 dB. Fig. 9 shows that when the third tone of 3.6 kHz is added from the low side, the two tonal peaks corresponding to 4kHz and 4.4 kHz are reduced. In Fig. 10, a third tone of 4.8 kHz is added instead from the high side, the two tonal peaks are also reduced but by a much smaller amount. Again we see the asymmetry of the low and high side suppression.

The three tone interaction is much less documented in the literature, here we shall compare our model results qualitatively with the experimental data on auditory neural response to multi-tones in [4]. Two tones are fixed at 4 kHz, 4.4 kHz, both at 50 dB. The third tone varies in frequency and in amplitude. In Fig. 11, we plot the BM response of two tones (4 kHz, plus line; 4.4 kHz, dotted line) as the third tone (line) increases its amplitude from 33 dB to 73 dB

for three values of frequencies, 3.6 kHz, 3.8 kHz, 4.2 kHz. We see that the two tone response decreases for increasing amplitude of third tone; and that the suppression effect on the 4kHz tone is larger at 3.8 kHz (low side) than at 4.2 kHz (high side) for the same amplitude of third tone. The effect of third tone at 3.6 kHz is even larger than that at 4.2 kHz. In Fig. 12, we plot similarly the response of two tones as the third tone takes on frequencies 4.3 kHz, 4.6 kHz, 4.8 kHz. The masking effect of third tone remains, except that the second tone at 4.4 kHz shows more difference as we observe the crossing of two tone curves when the frequency of third tone goes through that of the second tone (4.4 kHz). The third tone is more efficient in masking the second tone from the low side (4.3 kHz) than from the high side (4.6 kHz). The suppressing effect on the second tone is even weaker at 4.8 kHz. These features agree with those of Fig. 3 of Deng and Geisler [4], e.g. compare frame 4 and frame 6 there. Strictly speaking the neural data in [4] are synchrony masking responses, and BM responses we computed correspond to rate masking responses. However, their data are relevant for qualitative comparison, as there is close (positive) correlation between the rate and phase behavior, see [5].

5 Conclusions

We discussed the dispersive property of the cochlear models for time domain computation, and slow decay of long waves. A selective longitudinal damping term has been introduced in the nonlinear nonlocal model studied previously [2, 3]. The new model is computed using a semi-implicit second order finite difference method in the time domain. We presented numerical results on isodisplacement curves, two tone suppression, and three tone masking in qualitative agreement with earlier findings of Geisler [8] and experimental auditory neural data Deng and Geisler [4]. These encouraging results prompt one to perform further study of masking mechanism in more complex tones and speech input based on our cochlear model.

6 Acknowledgments

JX would like to thank Prof. C.D. Geisler for helpful email communications on two tone suppression and cochlear modeling.

References

- [1] Allen, J.B., Cochlear Modeling (1980, in Lecture Notes in Biomathematics, Springer-Verlag, 1980, eds. M. Holmes and L. Rubenfeld, volume 43, pp 1{8.
- [2] , de Boer, E., Mechanics of the Cochlear: Modeling Efforts, in Springer Handbook of Auditory Research, Springer-Verlag, 1996, eds. P. Dollas and A. Popper and R. Fay, volume 8, pp 258{317.
- [3] L. Deng, Processing of acoustic signals in a cochlear model incorporating laterally coupled suppressive elements, Neural Networks, 5 (1), pp 19{34, 1992.
- [4] L. Deng and C.D. Geisler, Responses of auditory-nerve fibers to multiple-tone complexes, J. Acoust. Soc. Amer., 82 (6), 1989{2000, 1987.
- [5] L. Deng and C.D. Geisler, Changes in the phase of excitor-tone responses in cat auditory-nerve fibers by suppressor tones and fatigue, J. Acoust. Soc. Amer, 78 (5), pp 1633{1643, 1985.
- [6] L. Deng and I. Keirallah, Numerical property and efficient solution of a transmission-line model for basilar membrane wave motions, Signal Processing, volume 33, pp 269{285, 1993.
- [7] R. Dijkstra, H. Duijhuys, H.W. Hoogstraten and M.A. Viergever, Numerical methods for solving one-dimensional cochlear models in the time domain, J. Acoust. Soc. Amer, 82 (5), pp 1655{1666, 1987.
- [8] Geisler, C.D., From Sound to Synapse, Oxford University Press, Oxford, 1998.
- [9] G. Golub and J. Ortega, Scientific Computing and Differential Equations, Academic Press, San Diego, CA, 1992.
- [10] J.J. Guinan and W.T. Peake, Middle-Ear Characteristics of Anesthetized Cats, J. Acoust. Soc. Amer, 41 (5), pp 1237{1261, 1967.
- [11] J.L. Hall, Two-tone suppression in a nonlinear model of the basilar membrane, J. Acoust. Soc. Amer, volume 61, pp 802{810, 1977.
- [12] Y. Jau and C.D. Geisler, Results from a cochlear model utilizing longitudinal coupling, in Mechanics of Hearing, Martinus Nijhoff Pub., Delft Univ. Press, 1983, E. de Boer and M. Viergever, pp 169{176.

- [13] Luc-J. Kanis and E. de Boer, Two-tone suppression in a locally active nonlinear model of the cochlear, *J. Acoust. Soc. Amer.*, 96(4), pp 2156{2165, 1994.
- [14] D. O. Kim, An overview of nonlinear and active models, in *Lecture Notes in Biomathematics: Peripheral Auditory Mechanisms*, Springer-Verlag, 1986, eds J. Allen and J.L. Hall and A. Hubbard and S.T. Neely and A. Tubis, volume 64, pp 239{249.
- [15] M. C. Liberman, The cochlear frequency map for the cat: Labeling auditory nerve fibers of known characteristic frequency, *J. Acoust. Soc. Amer.*, volume 72, pp 1441{1449, 1982.
- [16] Lighthill, J., Energy flow in the cochlear, *J. Fluid Mechanics*, volume 106, pp 149{213, 1981.
- [17] K-M Lim, Physical and Mathematical Cochlear Models, PhD Dissertation, Department of Mechanical Engineering, Stanford University, 2000.
- [18] B. Lutkenhoner and D. Jager, Stability of active cochlear models: need for a second tuned structure, in *Lecture Notes in Biomathematics: Peripheral Auditory Mechanisms*, Springer-Verlag, 1986, eds. J. Allen, J.L. Hall, A. Hubbard, S.T. Neely and A. Tubis, volume 64, pp 205{212.
- [19] R. Lyon, A computational model of filtering, detection, and compression in the cochlear, *IEEE International Conference on Acoustics, Speech and Signal Processing*, pp 1282{1285, 1982.
- [20] S. Neely, Mathematical modeling of cochlear mechanics, *J. Acoust. Soc. Amer.*, 78(1), pp 345{352, 1985.
- [21] W. S. Rhode, Observations of the vibration of the basilar membrane in the squirrel monkey using the Moossbauer techniques, *J. Acoust. Soc. Amer.*, volume 49, pp 1218{1231, 1971.
- [22] Sondhi, M., The Acoustical Inverse Problem for the Cochlear, *Lecture Notes in Biomathematics*, Springer-Verlag, 1980, eds M. Holmes and L. Rubenfeld, volume 43, pp 95{104.
- [23] J. Strikwerda, Finite Difference Schemes and Partial Differential Equations, Wadsworth and Brooks, Pacific Grove, CA, 1989.
- [24] von Békésy, G., *Experiments in Hearing*, McGraw-Hill, New York, 1960.

- [25] H. Wada, K. Ohyama, S. Noguchi and T. Takasaka, Generation mechanism of toneburst-evoked otoacoustic emissions: theoretical study, in *Biophysics of Hair-Cell Sensory Systems*, World Scientific, Singapore, 1993, eds H. Duifhuis, J. Horst, P. van Dijk, S.M. van Netten, pp 94-101.
- [26] G.B. Whitham, *Linear and Nonlinear Waves*, Wiley and Sons, New York, 1979.
- [27] J. Xin, Existence and Uniqueness of Traveling Waves in a Nonlinear Nonlocal Cochlear Model, in preparation, 2002.

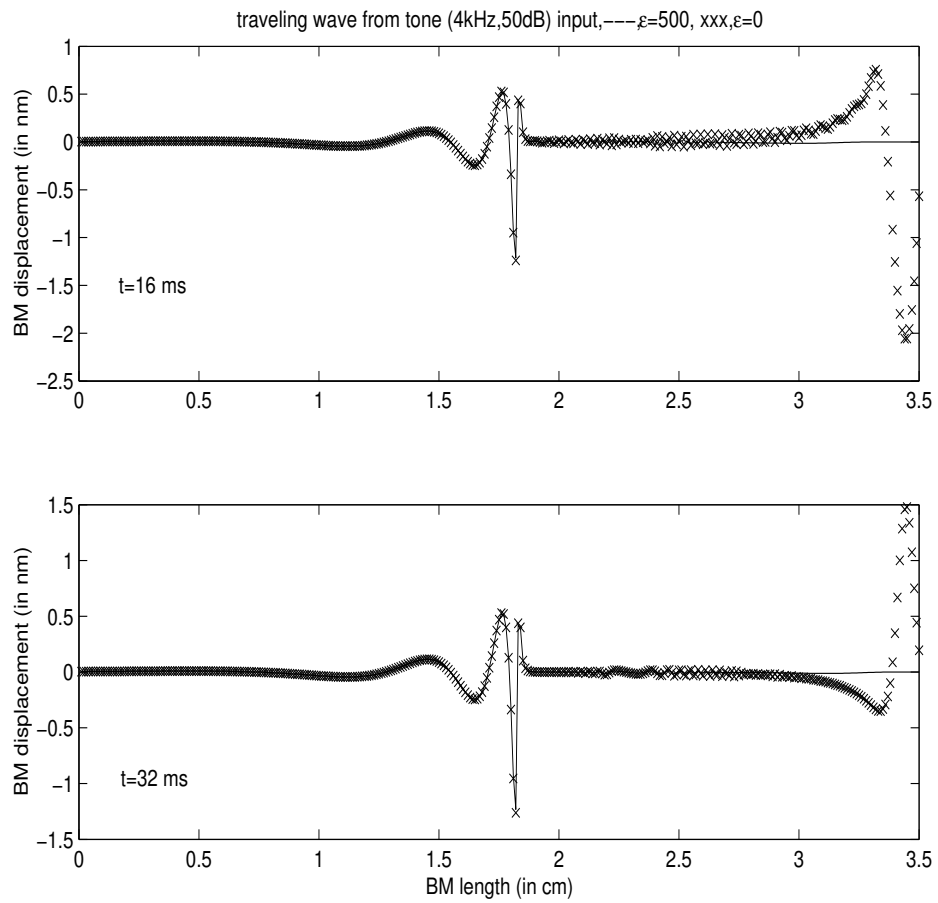


Figure 1: BM displacement at $t = 16$ ms (top) and $t = 32$ ms (bottom), from a (4kHz,50dB) input, w and w/o selective damping.

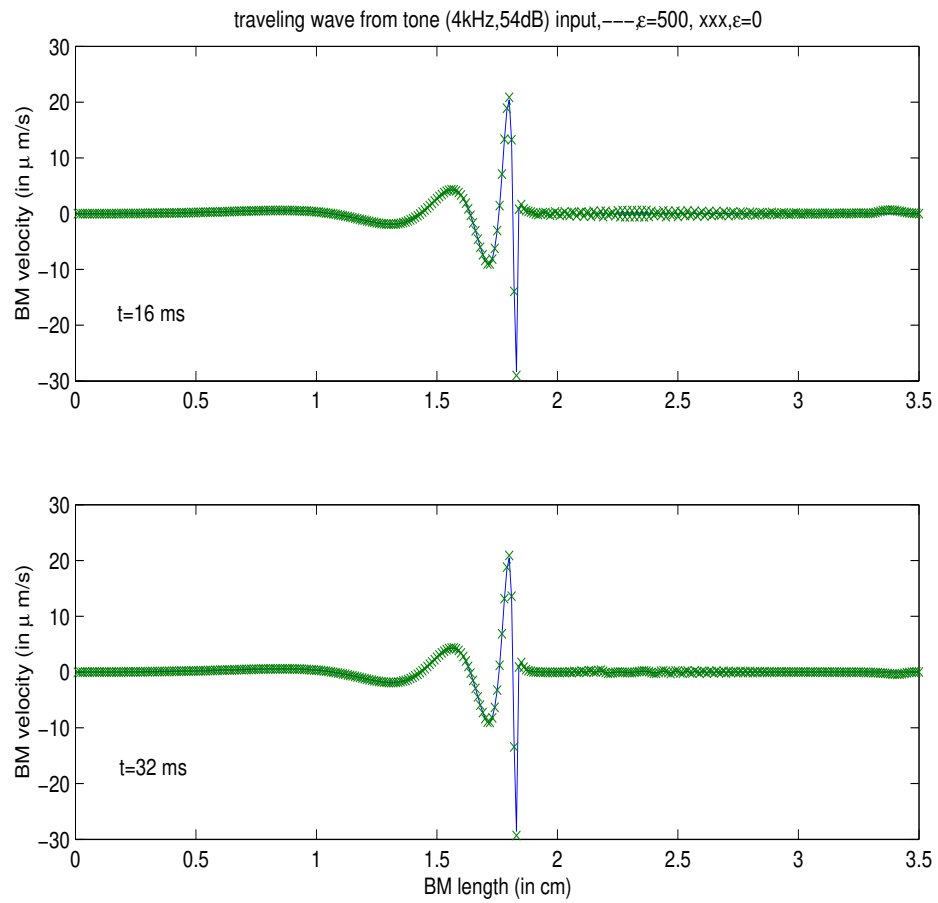


Figure 2: BM velocity at $t = 16$ ms (top) and $t = 32$ ms (bottom) from a (4kHz,50dB) input, w and w/o selective damping.

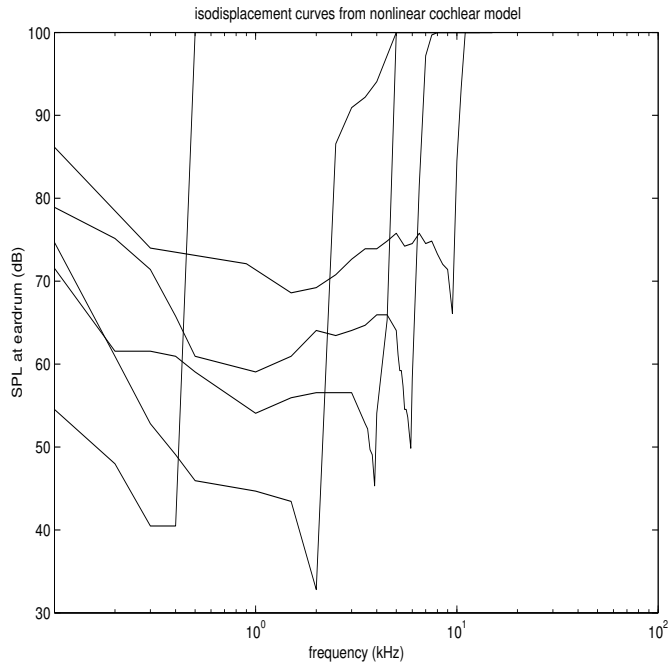


Figure 3: Isodisplacement curves (1 nm BM displacement) at various characteristic frequencies 500 Hz, 2 kHz, 4 kHz, 6 kHz, 10 kHz.

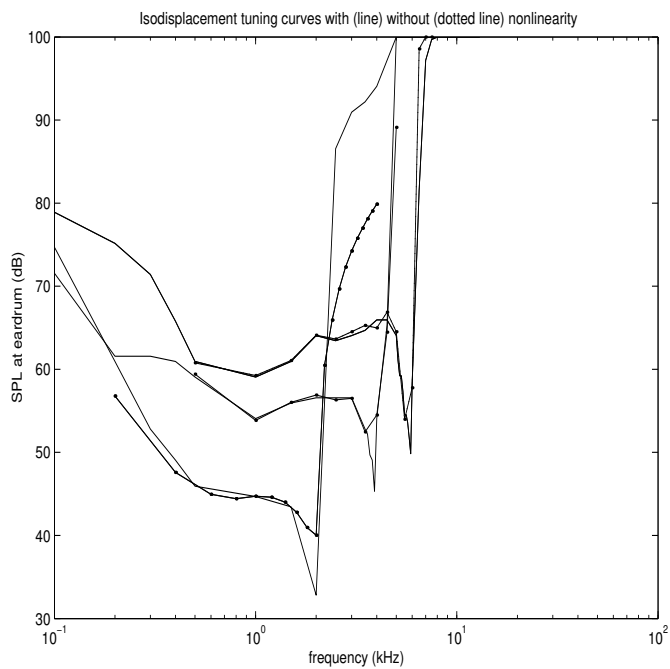


Figure 4: Isodisplacement curves (1 nm BM displacement) with/without nonlinearity at various characteristic frequencies 2 kHz, 4 kHz, 6 kHz.

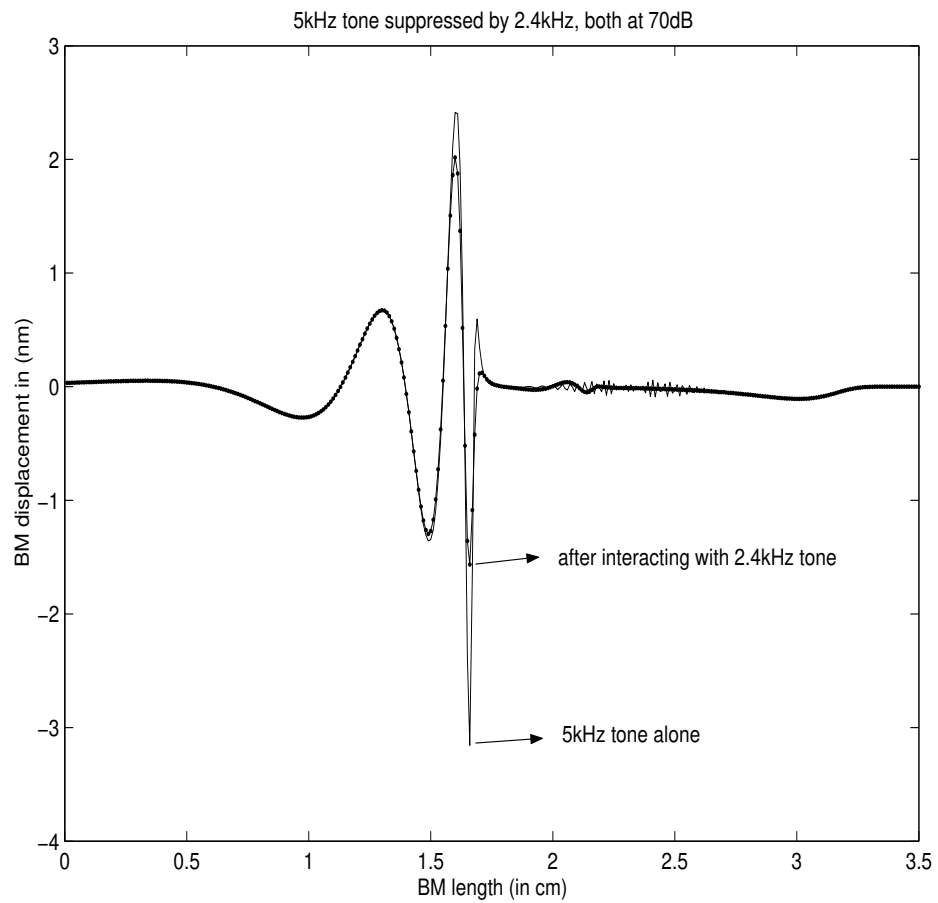


Figure 5: Low side masking effect of 2.4 kHz tone on 5kHz tone at 70 dB. Two tones dot{, 5kHz tone alone | .

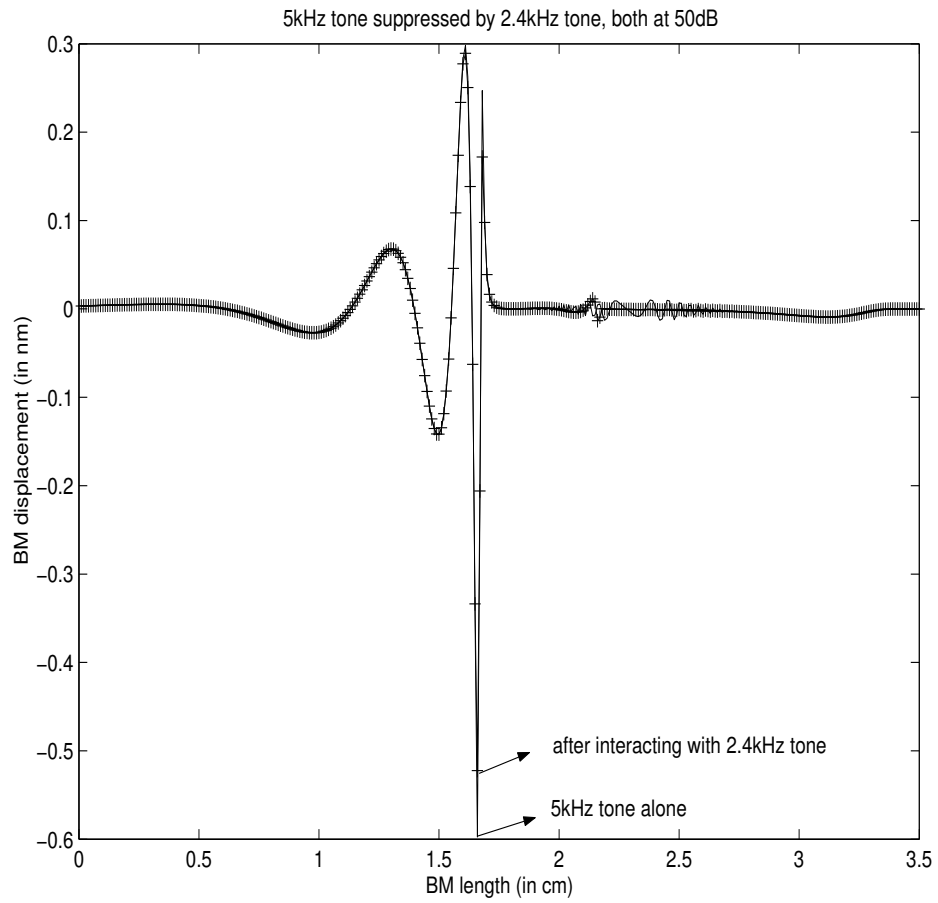


Figure 6: Low side masking effect of 2.4 kHz tone on 5kHz tone at 50 dB. Two tones + {, 5kHz tone alone | .

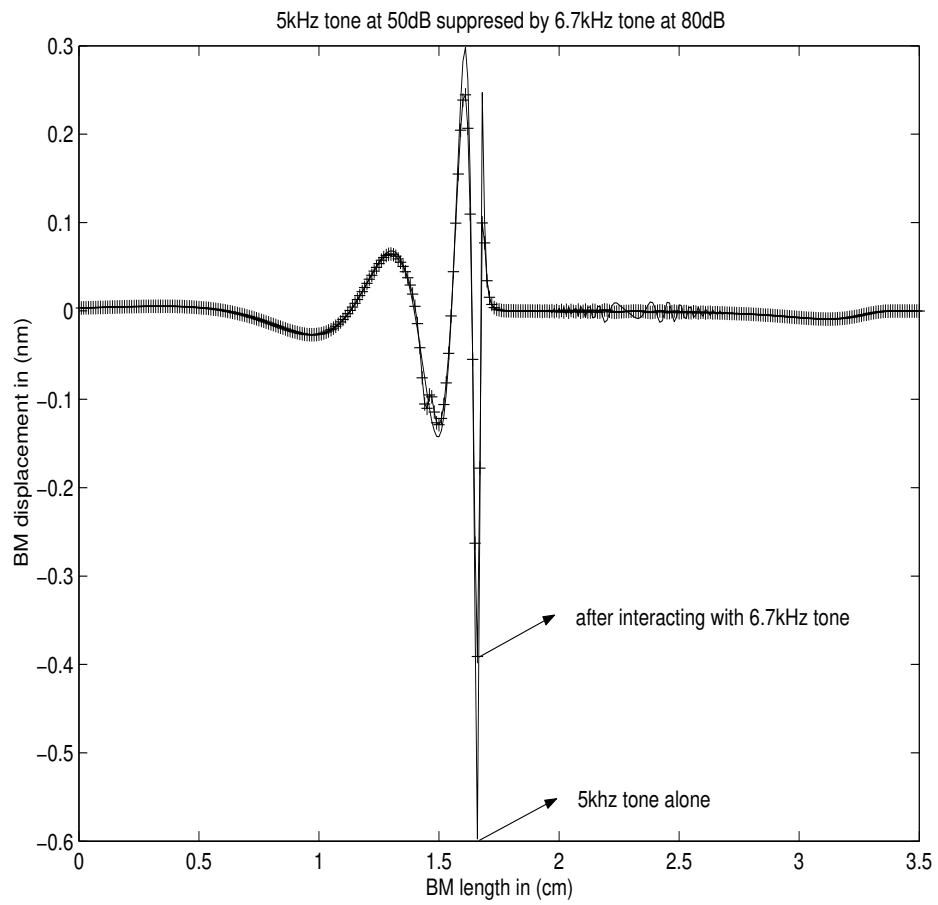


Figure 7: High side masking effect of 6.7 kHz tone on 5kHz tone at 80 dB. Two tones + {, 5kHz tone alone | .

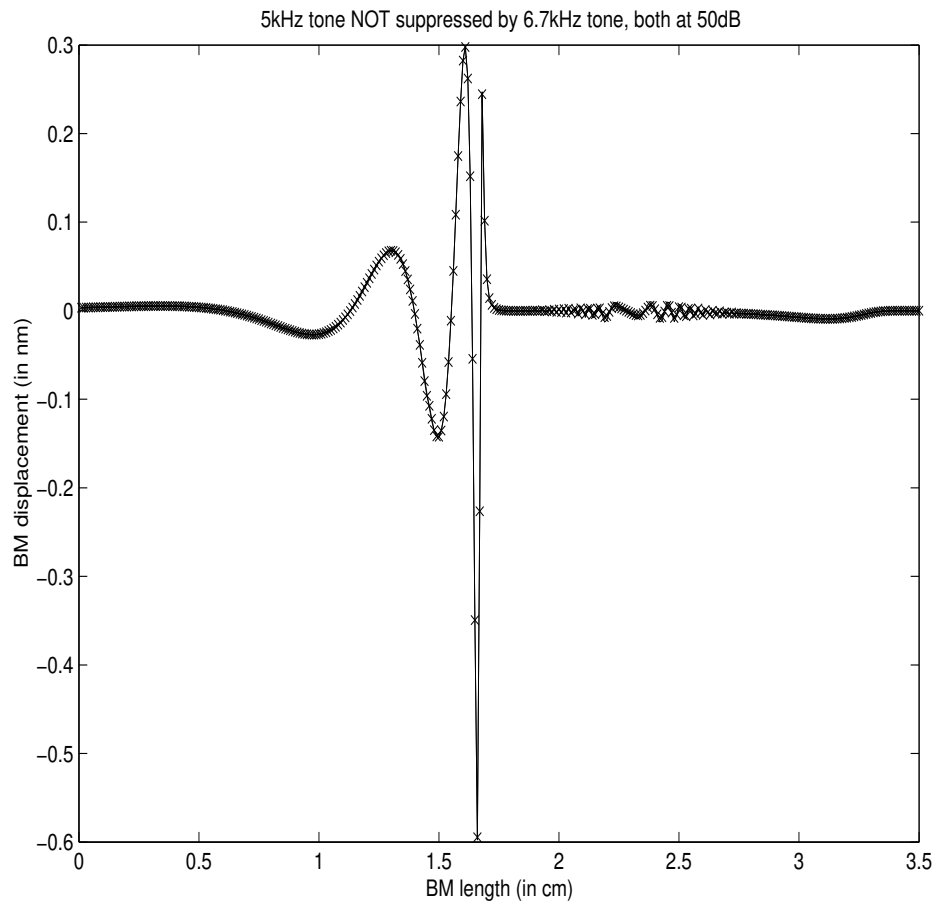


Figure 8: Absence of high side masking effect of 6.7 kHz tone on 5kHz tone at 50 dB. Two tones x{, 5kHz tone alone | .

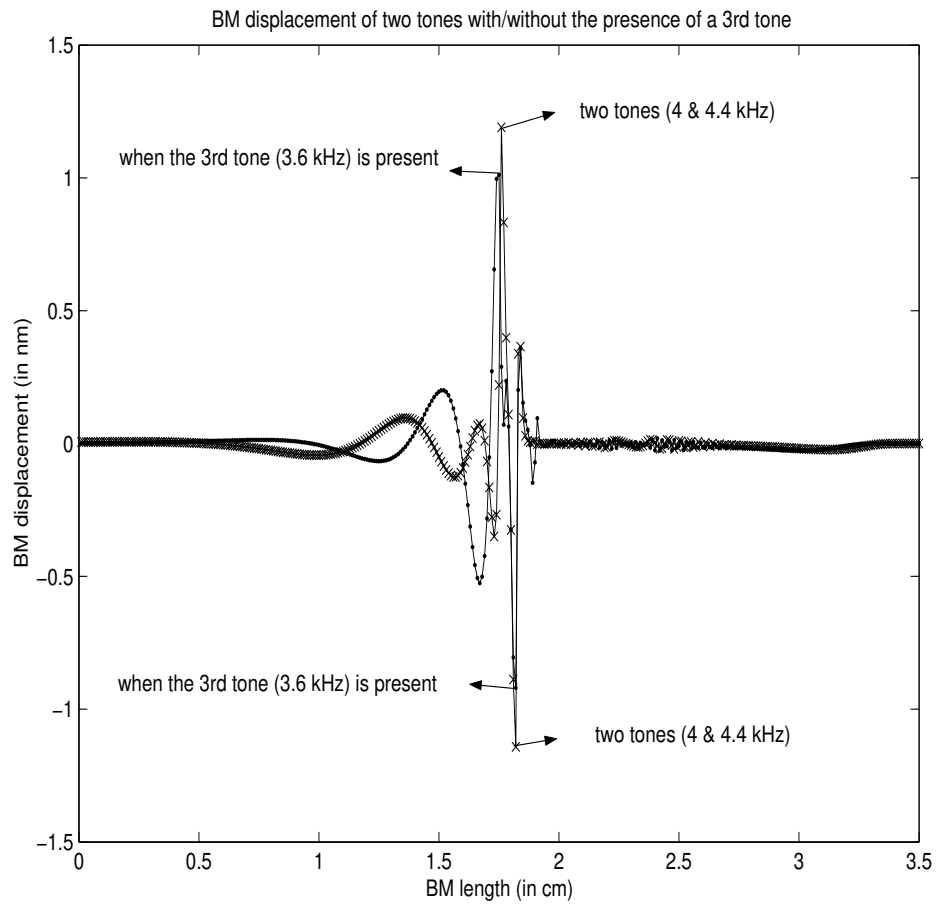


Figure 9: Low side masking effect of third tone 3.6 kHz on two tones (4 kHz, 4.4 kHz), all at 50 dB. Three tones dot, two tones x.

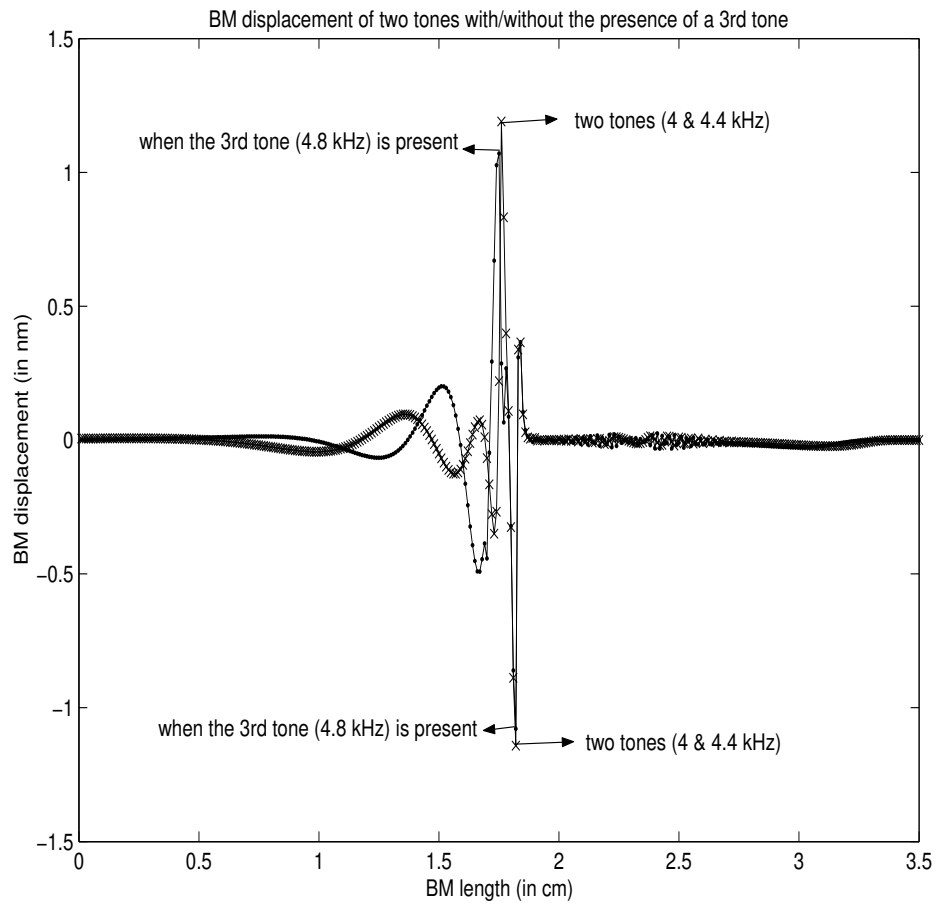


Figure 10: High side masking effect of third tone 4.8 kHz on two tones (4 kHz, 4.4 kHz), all at 50dB. Three tones dot, two tones x.

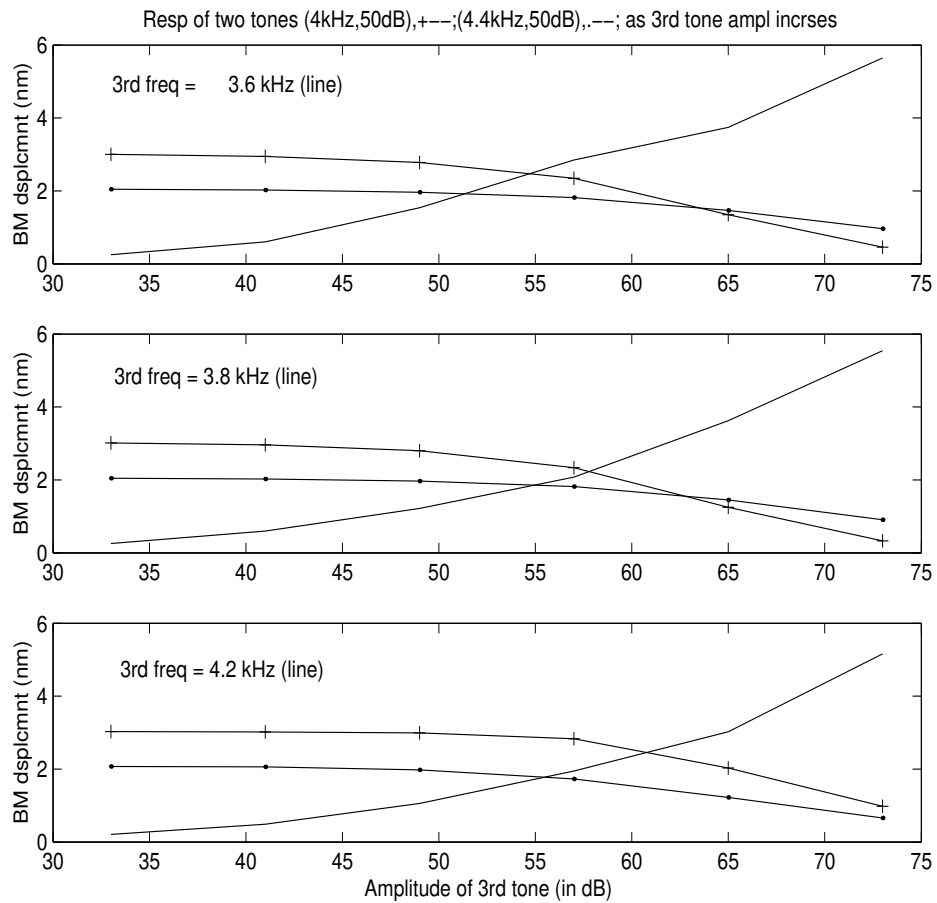


Figure 11: BM response of two tones (4 kHz, + ; 4.4 kHz, dot) as the third tone (|) increases its amplitude from 33 dB to 73 dB at three values of frequencies, 3.6 kHz, 3.8 kHz, 4.2 kHz.

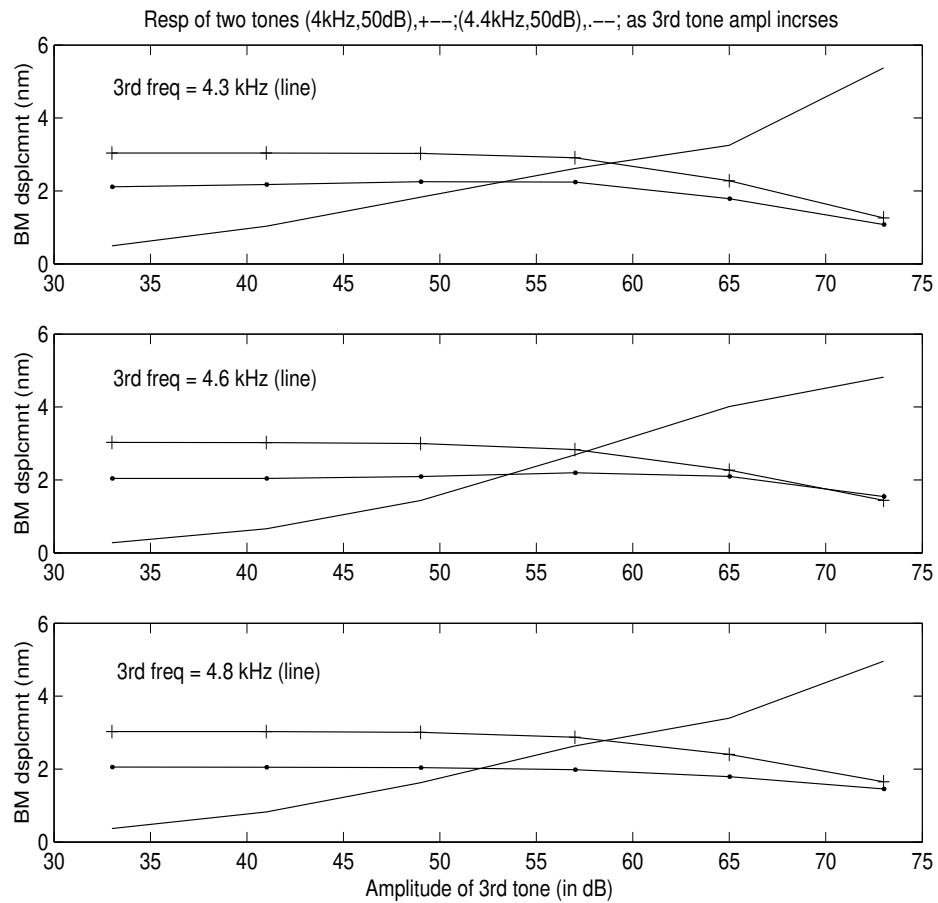


Figure 12: BM response of two tones (4 kHz, + ; 4.4 kHz, dot) as the third tone (|) increases its amplitude from 33 dB to 73 dB at three values of frequencies, 4.3 kHz, 4.6 kHz, 4.8 kHz.